Optica Applicata, Vol. LVI, No. 1, 2026
DOI: 10.37190/oa/215652

Propagation dynamics and radiation forces of Hermite non-uniformly correlated beams in tandem GRIN fiber

HONGJING LI, HANGHANG ZHANG*

Department of Mathematics and Physics, Luoyang Institute of Science and Technology, Luoyang 471023, China

*Corresponding author: hanghzhang@163.com

The propagation characteristics of Hermite non-uniformly correlated (HNUC) beams in axisymmetric gradient-index (GRIN) fibers were investigated, revealing the existence of dual focal points along the direction of optical transmission (z-axis) near $0.25L$ and $0.75L$. To exploit this bifocal property, tandem GRIN fibers were employed, with the dual foci positioned within the interstitial gap between the serially connected fibers. Through systematic analysis of the intensity distribution within the gap and the resulting radiation forces on Rayleigh particles, it was demonstrated that the HNUC beam establishes two stable equilibrium points along the z-axis within the gap region, both capable of three-dimensional optical trapping of Rayleigh particles. These findings suggest potential applications in fiber-optic tweezers systems for creating longitudinally distributed multiple optical potential wells.

Keywords: Hermite non-uniformly correlated beams, tandem gradient-index fiber, radiation forces, optical trapping.

1. Introduction

Light field manipulation has continued to be a prominent research focus in optics. In the spatial domain, it facilitates control not only over the amplitude distribution, phase structure, and polarization properties of optical fields but also over their spatial coherence for constructing structured light fields [1-3]. In recent years, through the design of coherence structures based on non-negative definiteness conditions, partially coherent (PC) beams with tailored spatial coherence structures have been shown to exhibit novel physical effects during propagation, including self-focusing, self-splitting, self-shifting, and self-shaping *etc.* [4-7]. These unique characteristics offer significant application potential in multiple domains, such as coherence-structured optical encryption, turbulence-resistant free-space optical communications, robust optical information transfer, and optical particle trapping/manipulation [8-11]. Since the seminal work by LAJUNEN *et al.* in 2011 that reported PC beams with non-uniform correlation (NUC) structures, extensive research has been conducted on various non-uniformly correlated beams, including Hermite-, Laguerre-, and Lorentz-type non-uniform coherence structured beams [11-13]. Each mode of these beams incorporates a quadratic phase factor, allowing for distinct focal positions for different modes. During propagation, different modes achieve dominance at specific distances. Furthermore, the weighting function in mode representation enables control over self-focusing properties, demonstrating remarkable potential for applications in particle manipulation.

Optical tweezers employ optical forces generated by the interaction of focused laser beams with microscopic particles, forming three-dimensional optical potential wells that enable precise manipulation of micro/nanoscale objects, including trapping, translation, and rotation [14-17]. Due to their high precision, non-contact operation, and minimal invasiveness, optical tweezers have been widely applied in single-cell manipulation, nanoparticle assembly, micro-force measurement, and biosensing [18-21]. As application domains continue to expand, the demands on optical manipulation capabilities have grown increasingly diverse. In recent years, fiber-based optical tweezers have emerged as a promising alternative owing to their low cost, ease of miniaturization and integration, as well as enhanced operational flexibility, which expands the movable range of trapped particles [22,23]. These advantages have facilitated significant applications in biochemical analysis and life sciences. Conventional fiber optical tweezers rely on tapered fiber probes. However, fabricating such probes remains technically challenging, and achieving precise control over the output optical field proves difficult. As a result, current fiber probes can generate only gradient optical fields with relatively simple structures, thereby limiting their manipulation capabilities. While applying the axisymmetric GRIN fiber to the fiber optic tweezers system, complex and diverse output optical field gradients are achieved by modulating the optical field structure of the incident beam.

In this study, the paper is organized as follows. Section 2 investigates the propagation characteristics of HNUC beams in both single and cascaded GRIN fibers based on the Collins integral formula. Section 3 employs the Rayleigh scattering theory to analyze the radiation forces exerted by HNUC beams on Rayleigh dielectric particles within the inter-fiber gap of tandem GRIN fiber configurations. Finally, the concluding remarks are presented in Section 4.

2. Propagation characteristics of HNUC beams in a GRIN fiber and cascaded GRIN fiber

For PC beams, the cross-spectral density (CSD) function is employed to characterize the statistical properties of the beam in the spatial-frequency domain. At the source plane ($z = 0$), the CSD function of a HNUC beam can be expressed as [13]

$$W_0(\mathbf{r}_1, \mathbf{r}_2, 0) = G_0 \exp\left(-\frac{\mathbf{r}_1^2 + \mathbf{r}_2^2}{w_0^2}\right) \mu_0(\mathbf{r}_1, \mathbf{r}_2) \tag{1}$$

where $\mathbf{r}_1 = (r_{1x}, r_{1y})$ and $\mathbf{r}_2 = (r_{2x}, r_{2y})$ represent the spatial coordinate vectors, G_0 is a constant related to the incident power, w_0 denotes the transverse beam width, and $\mu_0(\mathbf{r}_1, \mathbf{r}_2)$ represents the spatial coherence structure of the HNUC beam, which is expressed as

$$\mu_0(\mathbf{r}_1, \mathbf{r}_2) = \frac{1}{H_{2m}(0)} \exp\left[-\frac{(\mathbf{r}_2^2 - \mathbf{r}_1^2)^2}{\delta_0^4}\right] H_{2m}\left(\frac{\mathbf{r}_2^2 - \mathbf{r}_1^2}{\delta_0^2}\right) \tag{2}$$

where δ_0 denotes the coherence length of the HNUC beam, and H_{2m} represents the $2m$-order Hermite polynomial. When the beam order $m = 0$, the HNUC beam degenerates into the NUC beam.

The CSD function of the HNUC beam described previously can be derived through correspondence with a non-negative definite kernel, a condition that is satisfied if the function can be written in the following form

$$W_0(\mathbf{r}_1, \mathbf{r}_2) = \int p(v) V_0^*(\mathbf{r}_1, v) V_0(\mathbf{r}_2, v)\, \mathrm{d}v \tag{3}$$

where

$$p(v) = (4\pi)^{-1/2} \left(\frac{2}{\gamma}\right)^{2m+1} v^{2m} \exp\left(-\frac{v^2}{\gamma^2}\right) \tag{4}$$

$$V_0(\mathbf{r}, v) = \exp\left(-\frac{\mathbf{r}^2}{w_0^2}\right) \exp(-ikv\mathbf{r}^2) \tag{5}$$

in which $p(v)$ represents a weighting function, $V_0(\mathbf{r}, v)$ serves as the kernel function, $k = 2\pi/\lambda$ is the wavenumber, and λ denotes the wavelength. By substituting Eqs. (4) and (5) into Eq. (3), the CSD function of HNUC beams can be obtained through straightforward integration.

The propagation of the HNUC beam through single GRIN fiber and cascaded GRIN fiber systems is considered, as illustrated in Fig. 1(a) and (b), respectively. The ABCD transfer matrix relating the input plane ($z = 0$) to the output plane z in Fig. 1(a) is given by

$$\begin{bmatrix} A_1 & B_1 \\ C_1 & D_1 \end{bmatrix}_z = \begin{bmatrix} \cos(\beta z) & \dfrac{\sin(\beta z)}{n_0 \beta} \\ -n_0 \beta \sin(\beta z) & \cos(\beta z) \end{bmatrix} \tag{6}$$

where A_1, B_1, C_1, and D_1 denote the transfer matrix elements of the single GRIN fiber, z represents the distance between the input plane and the target plane, n_0 denotes the refractive-index of the symmetry axis (*i.e.*, z-axis), and β is the distribution factor of the refractive index of the GRIN fiber. Light propagation in a GRIN fiber exhibits pe-

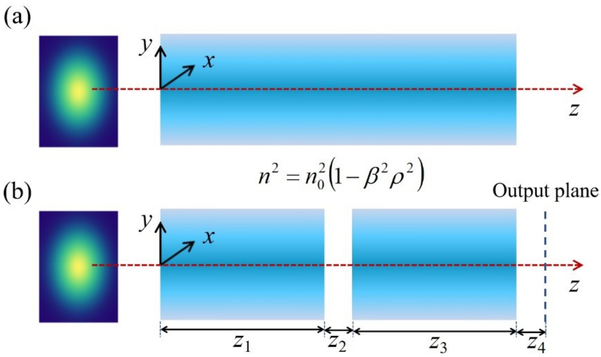

Fig. 1. Illustration of the propagation of a HNUC beam in a GRIN fiber (a) and cascaded GRIN fiber (b).

riodic behavior. The period length equals $L/2$, where $L = 2\pi/\beta$. The transfer matrix in Fig. 1(b) can be written in the following form

$$\begin{bmatrix} A_2 & B_2 \\ C_2 & D_2 \end{bmatrix}_z = \begin{bmatrix} 1 & z_4 \\ 0 & 1 \end{bmatrix} \begin{bmatrix} \cos(\beta z_3) & \dfrac{\sin(\beta z_3)}{n_0\beta} \\ -n_0\beta\sin(\beta z_3) & \cos(\beta z_3) \end{bmatrix} \begin{bmatrix} 1 & z_2 \\ 0 & 1 \end{bmatrix} \begin{bmatrix} \cos(\beta z_1) & \dfrac{\sin(\beta z_1)}{n_0\beta} \\ -n_0\beta\sin(\beta z_1) & \cos(\beta z_1) \end{bmatrix} \tag{7}$$

where A_2, B_2, C_2, and D_2 denote the transfer matrix elements of the cascaded GRIN fiber systems, z_1 and z_3 correspond to the lengths of the first and second GRIN fiber segments, respectively, while z_2 and z_4 represent the lengths of the GRIN fiber gaps.

We study the propagation of HNUC beams in a GRIN fiber with a radial distribution of refractive index. To quantify this distribution, the refractive index profile of the GRIN fiber follows a parabolic distribution, which can be expressed as

$$n^2 = \begin{cases} n_0^2(1-\beta^2\rho^2), & \rho^2 < R_0^2 \\ n_0^2(1-\beta^2 R_0^2), & \rho^2 \geq R_0^2 \end{cases} \tag{8}$$

where $\rho = |\boldsymbol{\rho}|$ denotes the radial distance from the z-axis to a point within the cross -section, R_0 represents the core radius of the GRIN fiber, and distribution factor $\beta^2 = (1 - n_1^2/n_0^2)/R_0^2$, where n_1 is the refractive index at the fiber boundary.

Within the framework of the Collins formula and under the paraxial approximation [24], the CSD function of the HNUC beam propagating through an ABCD optical system can be expressed as

$$W(\boldsymbol{\rho}_1, \boldsymbol{\rho}_2, z) = \left(\frac{1}{\lambda B}\right)^2 \iiiint W_0(\mathbf{r}_1, \mathbf{r}_2, 0) \exp\left[-\frac{ikD}{2B}(\boldsymbol{\rho}_1^2 - \boldsymbol{\rho}_2^2)\right]$$
$$\times \exp\left[-\frac{ikA}{2B}(\mathbf{r}_1^2 - \mathbf{r}_2^2) + \frac{ik}{B}(\mathbf{r}_1 \cdot \boldsymbol{\rho}_1 - \mathbf{r}_2 \cdot \boldsymbol{\rho}_2)\right] \mathrm{d}^2\mathbf{r}_1 \mathrm{d}^2\mathbf{r}_2 \tag{9}$$

where $\boldsymbol{\rho}_1 = (\rho_{1x}, \rho_{1y})$ and $\boldsymbol{\rho}_2 = (\rho_{2x}, \rho_{2y})$ correspond to the position vectors in the output plane, while A, B, and D denote the transfer matrix elements of the optical system.

The CSD function of the HNUC beam in the output plane could be calculated by substituting Eqs. (1) and (2) into Eq. (9). However, the presence of higher-order terms renders the integration of Eq. (9) analytically intractable. Therefore, by substituting Eqs. (3)–(5) into Eq. (9) and performing the necessary integration, the expression for the CSD function of the HNUC beam via an ABCD optical system turns out to be

$$W(\boldsymbol{\rho}_1, \boldsymbol{\rho}_2, z) = \int p(v) P(\boldsymbol{\rho}_1, \boldsymbol{\rho}_2, v, z) \mathrm{d}v \tag{10}$$

where $\mathrm{P}(\boldsymbol{\rho}_1, \boldsymbol{\rho}_2, v, z)$ is defined as

$$P(\boldsymbol{\rho}_1, \boldsymbol{\rho}_2, v, z) = \left(\frac{1}{\lambda B}\right)^2 \iiiint V_0^*(\mathbf{r}_1, v) V_0(\mathbf{r}_2, v) \exp\left[-\frac{ikD}{2B}(\boldsymbol{\rho}_1^2 - \boldsymbol{\rho}_2^2)\right]$$
$$\times \exp\left[-\frac{ikA}{2B}(\mathbf{r}_1^2 - \mathbf{r}_2^2) + \frac{ik}{B}(\mathbf{r}_1 \cdot \boldsymbol{\rho}_1 - \mathbf{r}_2 \cdot \boldsymbol{\rho}_2)\right] \mathrm{d}^2\mathbf{r}_1 \mathrm{d}^2\mathbf{r}_2 \tag{11}$$

by substituting Eq. (5) into Eq. (11), after integrating over $\mathbf{r}_1(r_{1x}, r_{1y})$ and $\mathbf{r}_2(r_{2x}, r_{2y})$, $P(\boldsymbol{\rho}_1, \boldsymbol{\rho}_2, v, z)$ is obtained as

$$P(\boldsymbol{\rho}_1, \boldsymbol{\rho}_2, v, z) = \frac{G_0 \pi^2}{M_1 M_2 \lambda^2 B^2} \exp\left[-\frac{ikD}{2z}(\boldsymbol{\rho}_1^2 - \boldsymbol{\rho}_2^2)\right] \exp\left(-\frac{k^2 \boldsymbol{\rho}_1^2}{4B^2 M_1} - \frac{k^2 \boldsymbol{\rho}_2^2}{4B^2 M_2}\right) \tag{12}$$

in which

$$M_1 = \frac{1}{w_0^2} - ikv + \frac{ikA}{2B}, \qquad M_2 = \frac{1}{w_0^2} + ikv - \frac{ikA}{2B} \tag{13}$$

Based on the relation $I(\boldsymbol{\rho}, z) = W(\boldsymbol{\rho}, \boldsymbol{\rho}, z)$ between the intensity $I(\boldsymbol{\rho}, z)$ and the CSD function $W(\boldsymbol{\rho}, \boldsymbol{\rho}, z)$ at any point of the output plane, the expression for the intensity distribution of the HNUC beam in a single GRIN fiber is derived by substituting Eqs. (6), (12), and (13) into Eq. (10), yielding

$$I(\boldsymbol{\rho}, z) = \int p(v) \frac{G_0 \pi^2}{M_1 M_2 \lambda^2 B_1^2} \exp\left(-\frac{k^2 \boldsymbol{\rho}^2}{4B_1^2 M_1} - \frac{k^2 \boldsymbol{\rho}^2}{4B_1^2 M_2}\right) \mathrm{d}v \tag{14}$$

Similarly, the expression for the intensity distribution in cascaded GRIN fibers is derived by substituting Eqs. (6), (12), and (13) into Eq. (10), resulting in

$$I(\boldsymbol{\rho}, z) = \int p(v) \frac{G_0 \pi^2}{M_1 M_2 \lambda^2 B_2^2} \exp\left(-\frac{k^2 \boldsymbol{\rho}^2}{4B_2^2 M_1} - \frac{k^2 \boldsymbol{\rho}^2}{4B_2^2 M_2}\right) \mathrm{d}v \tag{15}$$

These expressions are used to study the propagation properties of HNUC beams in single and cascaded GRIN fiber systems through detailed numerical calculations. The parameters values employed in calculations are $P = 1$ W, $\lambda = 632.8$ nm, $n_0 = 1.49$, $n_1 = 1.45$, $w_0 = 200/k$, and $\delta_0 = 200/k$, unless otherwise stated in the text.

The intensity distribution of the HNUC beam in the GRIN fiber for different values of the beam order is given in Fig. 2. The white line indicates the axial intensity distribution (along the z-axis). From the figure, it can be seen the process of periodic focusing

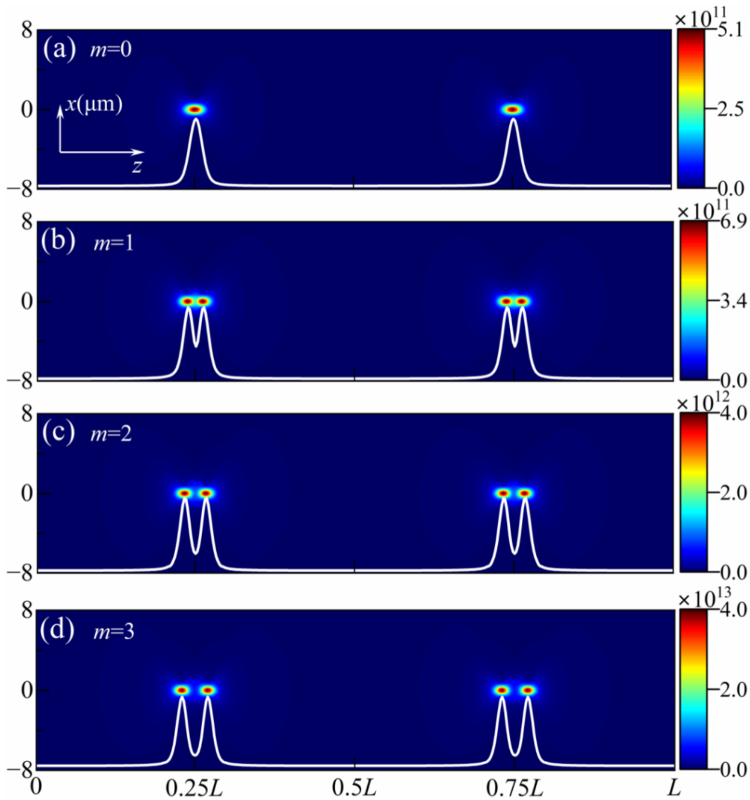

Fig. 2. Intensity distribution for different beam order m along the x-z plane within a GRIN fiber with a parabolic refractive-index, (a) $m = 0$, (b) $m = 1$, (c) $m = 2$, and (d) $m = 3$.

and reconstruction of the HNUC beam, which is a property given to the beam by the GRIN fiber with a parabolic refractive-index. For beam order $m = 0$, the HNUC beam propagation characteristics resemble those of perfect vortex and Lommel beams in the GRIN fiber [25,26], exhibiting focal points at $0.25L$ and $0.75L$. For the beam order $m > 0$, the HNUC beam has two focal points (intensity maxima) at approximately $0.25L$ and $0.75L$ along the z-axis. This indicates that the HNUC beam undergoes the process of focusing, divergence and refocusing within a short distance near $0.25L$ and $0.75L$ during its interaction with the GRIN fiber, which may be due to the strong self -focusing property of the HNUC beam in this case. Furthermore, increasing the beam order enhances both the peak intensity and the separation between the two focal points near $0.25L$ and $0.75L$.

To exploit the bifocal distribution near $0.25L$ and $0.75L$ along the propagation axis, a cascaded GRIN fiber configuration (Fig. 1(b)) is employed, positioning the bifocal region between the two GRIN fiber segments. The intensity distribution of the HNUC beam in the gap of the cascaded GRIN fiber is given in Fig. 3, with the beam

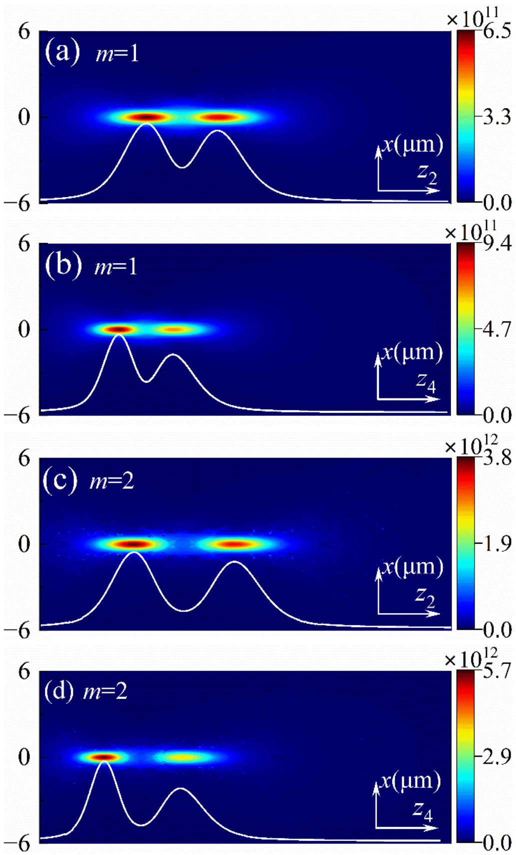

Fig. 3. Intensity distribution of the HNUC beam in the gap of the cascaded GRIN fiber, (a) and (b) $m = 1$, (c) and (d) $m = 2$.

order $m = 1$ in Figs. (a) and (b), the beam order $m = 2$ in Figs. (c) and (d), z_2 region in the cascaded GRIN fiber (Fig. 1(b)) in Figs. (a) and (c), and z_4 region in the cascaded GRIN fiber in Figs. (b) and (d). The system parameters are set as $z_1 = L/5$, $z_2 = L/10$, $z_3 = 3L/8$, and $z_4 = L/10$. From the figures, it can be seen that the bifocal point distribution persists in the gap regions along the direction of beam propagation, with the rear focus intensity being lower than the front focus, and the peak intensity in z_4 region exceeding that in z_2 region. Compared with Fig. 2, the cascaded GRIN fiber configuration yields higher intensity maxima when focusing HNUC beams of the same order.

3. Radiation forces exerted by HNUC beams

When light interacts with a microparticle and becomes scattered, momentum exchange takes place between photons and the particle, resulting in optical radiation pressure. Under the assumption that the dielectric particle radius is significantly smaller than the incident light wavelength ($a_0 \ll \lambda$), the system can be described by the Rayleigh scattering regime, where the particle is approximated as a point dipole.

According to the Rayleigh scattering theory, the gradient force $\mathbf{F}_{\text{Grad}}$ scales with the electric field intensity gradient, expressed as [27,28]

$$\mathbf{F}_{\text{Grad}} = \frac{1}{4}\text{Re}(\alpha)\nabla\left|E(\rho_x, \rho_y, z)\right|^2 \tag{16}$$

where $\left|E(\rho_x, \rho_y, z)\right|^2 = 2I(\rho_x, \rho_y, z)/(n_m \varepsilon_0 c)$, $I(\rho_x, \rho_y, z)$ corresponds to the intensity of the HNUC beam in the target plane, n_m is the host medium refractive index, ε_0 represents the vacuum permittivity, and c is the speed of light in vacuum. The real part of the particle polarizability, $\text{Re}(\alpha)$, is given by

$$\alpha = \frac{\alpha_0}{1 - i\alpha_0 k^3/(6\pi\varepsilon_0)} \tag{17}$$

where $\alpha_0 = 4\pi\varepsilon_\text{m} a_0^3(\varepsilon_\text{p} - \varepsilon_\text{m})/(\varepsilon_\text{p} + 2\varepsilon_\text{m})$, with ε_p and ε_m denote the relative permittivities of the particle and the host medium, respectively. The permittivity-refractive index relation is given by $\varepsilon_i = n_i^2$ (where $i = p$ or m). The scattering force $\mathbf{F}_{\text{Scat}}$ is proportional to the light intensity values and is along the z-direction (the direction of light propagation), which can be expressed in the following form [27,28]

$$\mathbf{F}_{\text{Scat}} = \mathbf{e}_z \frac{n_\text{m}}{c} C_{\text{Scat}} I(\rho_x, \rho_y, z) \tag{18}$$

where $\mathbf{e}_z$ is a unit vector along the beam propagation direction, and $C_{\text{Scat}} = k_0^4|\alpha|^2/(6\pi\varepsilon_0^2)$ denotes the scattering cross-section of the Rayleigh particle. Substitution of Eq. (15) into Eqs. (16) and (18) enables the calculation of the gradient and scattering forces on a Rayleigh dielectric particle exerted by an HNUC beam in the gap region of cascaded GRIN fibers. The gradient force $\mathbf{F}_{\text{Grad}}$ includes the transverse gradient force $\mathbf{F}_{\text{Grad},x}$ ($\mathbf{F}_{\text{Grad},y}$) along the ρ_x-ρ_y plane, as well as the longitudinal gradient force $\mathbf{F}_{\text{Grad},z}$ along the z-direction. It can be found that the direction of the longitudinal gradient force $\mathbf{F}_{\text{Grad},z}$ and the direction of the scattering force $\mathbf{F}_{\text{Scat}}$ are both along the z-axis, so the sum of longitudinal gradient force and scattering force, *i.e.*, $\mathbf{F}_{\text{Grad},z} + \mathbf{F}_{\text{Scat}}$, represents the resultant force along the z-axis, referred to as the longitudinal radiation force.

The variations of the radiation forces exerted by the focused HNUC beam on the Rayleigh particles in the z_2 region are depicted in Fig. 4, where $m = 2$, $n_\text{m} = 1$, $n_\text{p} = 1.592$ (*i.e.*, glass), $a_0 = 30$ nm, with all other calculation parameters consistent with those in Fig. 3. Figure 4(a) illustrates the transverse gradient force $\mathbf{F}_{\text{Grad},x}$ at the front focus and back focus cross-sections. Figure 4(b) depicts the longitudinal gradient force $\mathbf{F}_{\text{Grad},z}$. Figure 4(c) presents the scattering force $\mathbf{F}_{\text{Scat}}$. Figure 4(d) demonstrates the sum of longitudinal gradient force and scattering force $\mathbf{F}_{\text{Grad},z} + \mathbf{F}_{\text{Scat}}$ along the z-axis. The force sign convention is defined as follows: positive the transverse gradient force $\mathbf{F}_{\text{Grad},x}$ corresponds to $+\rho_x$ direction, while negative values indicate $-\rho_x$ direction; similarly, the longitudinal gradient force $\mathbf{F}_{\text{Grad},z} > 0$ denotes $+z$ direction and $\mathbf{F}_{\text{Grad},z} < 0$ indicates $-z$ direction.

As illustrated in Figs. 4(a)–(d), it can be observed that the direction of the transverse gradient forces $\mathbf{F}_{\text{Grad},x}$ points to $\rho_x = 0$ μm at both the front focus and back focus cross-sections, indicating that in both focal planes, the transverse gradient force drives

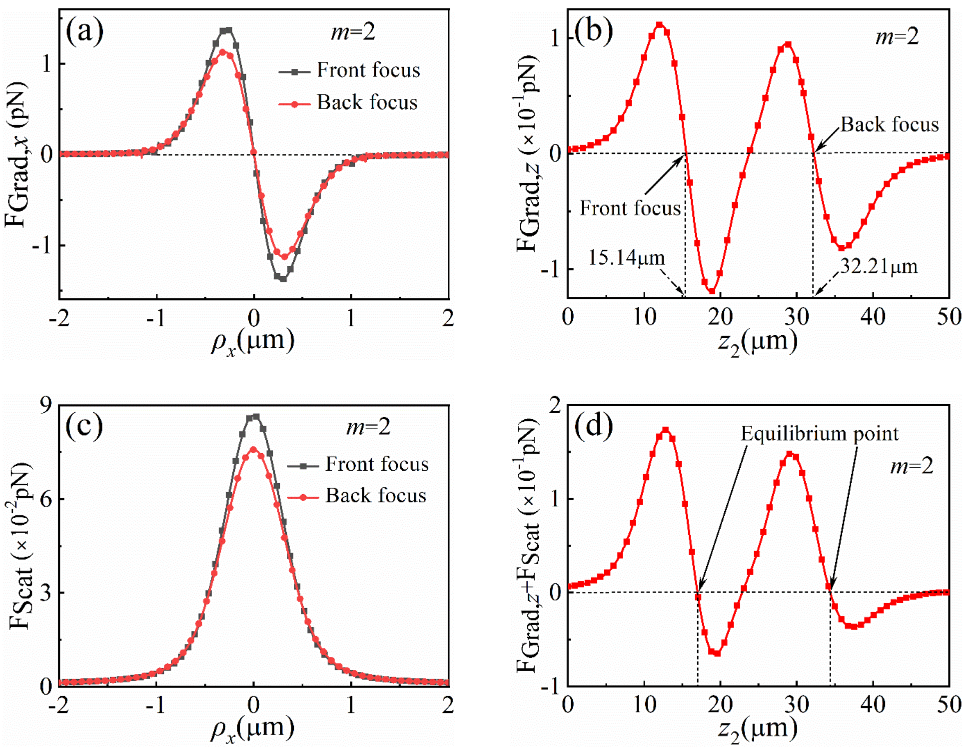

Fig. 4. Radiation forces on Rayleigh particles from the HNUC beam in the z_2 region, (a) $\mathbf{F}_{\text{Grad},x}$, (b) $\mathbf{F}_{\text{Grad},z}$, (c) $\mathbf{F}_{\text{Scat}}$, (d) $\mathbf{F}_{\text{Grad},z} + \mathbf{F}_{\text{Scat}}$.

the particle toward the focus. The direction of longitudinal gradient force $\mathbf{F}_{\mathrm{Grad},z}$ points to $z_2 = 15.14$ μm (the front focal point) and $z_2 = 32.21$ μm (the back focal point), demonstrating in the z-axis direction, the longitudinal gradient force drives the particles towards these two points. In addition, the scattering force is numerically smaller than the longitudinal gradient force, *i.e.*, the longitudinal gradient force is able to overcome the forward scattering force, indicating that the particles can be stably captured along the z-axis. Therefore, both the front and back focuses can capture Rayleigh particles stably in three dimensions in the z_2 region.

The radiation force of the HNUC beam on the Rayleigh particles in the z_4 region is given in Fig. 5, and the calculated parameters are the same as those in Figs. 3 and 4. From the figure, it can be seen that the HNUC beam has two stable equilibrium points distributed along the z-axis in the z_4 region, both of which can capture the Rayleigh particles in three dimensions. Compared with the z_2 region in Fig. 4, the difference in the magnitude of the radiation force between the front and back foci is much larger, and the radiation force at the front focus is about twice as large as that at the back focus in the z_4 region.

The trapping stability is discussed next. For three-dimensional stable optical trapping to be achieved, three conditions must be satisfied simultaneously: (1) Stable con-

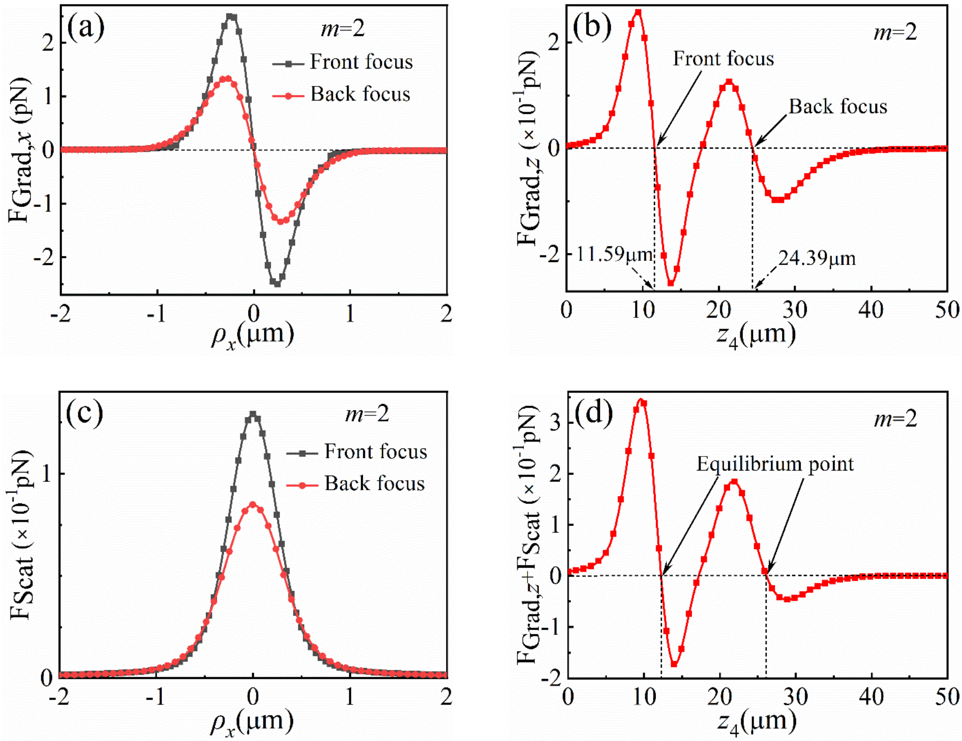

Fig. 5. Radiation forces of the HNUC beam on Rayleigh particles in the z_4 region, (a) $\mathbf{F}_{\mathrm{Grad},x}$, (b) $\mathbf{F}_{\mathrm{Grad},z}$, (c) $\mathbf{F}_{\mathrm{Scat}}$, (d) $\mathbf{F}_{\mathrm{Grad},z} + \mathbf{F}_{\mathrm{Scat}}$.

finement in the transverse plane, which is met as the transverse gradient force fulfills this requirement, as evidenced in Figs. 4(a) and 5(a). (2) Stable trapping along the z-axial direction, which requires that the longitudinal gradient force overcomes the scattering force. This condition is satisfied, as shown in Figs. 4(d) and 5(d), where the longitudinal gradient force exceeds the scattering force. (3) Both the transverse and longitudinal gradient forces must be sufficient to overcome the influence of Brownian motion. The Brownian force is defined as $F_{\mathrm{B}} = (12\pi\eta a_0 k_{\mathrm{b}} T)^{1/2}$ [29], where η denotes the viscosity of the ambient medium, with a value of $\eta = 7.977 \times 10^{-4}$ Pa·s for water at a temperature $T = 300$ K, and k_{b} is the Boltzmann constant. The calculation shows that the Brownian force is equal to 1.9355×10^{-3} pN, which is significantly smaller than both the transverse and longitudinal gradient forces. Therefore, three-dimensional stable trapping of Rayleigh particles by the HNUC beam can be achieved at these stable equilibrium points.

4. Conclusions

In this paper, we investigate the propagation characteristics of HNUC beams in both single and cascaded GRIN fibers based on the Collins integral formula and Rayleigh scattering theory, with particular focus on the radiation forces exerted on Rayleigh particles within the inter-fiber gap of tandem GRIN fiber configurations. The results reveal that HNUC beams exhibit periodic focusing and reconstruction in GRIN fibers, demonstrating dual focal points along the z-axis at approximately $0.25L$ and $0.75L$ positions. To exploit this bifocal property, a cascaded GRIN fiber system was designed to position both foci within the inter-fiber gap. Notably, two axial intensity maxima are maintained in the gap region, where the anterior focal point exhibiting greater peak intensity than the posterior focal point. Theoretical analysis confirms that HNUC beams can achieve three-dimensional stable trapping of Rayleigh particles at both axially separated focal positions. These findings suggest potential applications in fiber-based optical tweezers systems, particularly for scenarios requiring multiple trapping zones along the optical axis. The demonstrated ability to maintain dual trapping potentials within an engineered fiber gap could enable novel manipulation schemes in microfluidics and biophotonics applications.

Funding
This work was supported by the Major Science and Technology Special Project of Henan Province (Grant No. 251100210200) and the Key Research Projects of Colleges and Universities in Henan Province (Grant No. 26B140008).

Declaration of competing interest
The authors declare that they have no known competing financial interests or personal relationships that could have appeared to influence the work reported in this paper.

Data availability
Data will be made available on request.

References

[1] FORBES A., DE OLIVEIRA M., DENNIS M.R., *Structured light*, Nature Photonics, **15**(4), 2021: 253-262. https://doi.org/10.1038/s41566-021-00780-4

[2] ZHAN Q., *Spatiotemporal sculpturing of light: A tutorial*, Advances in Optics Photonics, **16**(2), 2024: 163-228. https://doi.org/10.1364/AOP.507558

[3] DORRAH A.H., CAPASSO F., *Tunable structured light with flat optics*, Science, **376**(6591), 2022: eabi6860. https://doi.org/10.1126/science.abi6860

[4] CHEN Y., WANG F., CAI Y., *Partially coherent light beam shaping via complex spatial coherence structure engineering*, Advances in Physics: X, **7**(1), 2022: 2009742. https://doi.org/10.1080/23746149.2021.2009742

[5] YU J., ZHU X., WANG F., CHEN Y., CAI Y., *Research progress on manipulating spatial coherence structure of light beam and its applications*, Progress in Quantum Electronics, **91-92**, 2023: 100486. https://doi.org/10.1016/j.pquantelec.2023.100486

[6] LIU Y., DONG Z., WANG F., CHEN Y., CAI Y., *Generation of a higher-order Poincaré sphere beam array with spatial coherence engineering*, Optics Letters, **47**(19), 2022: 5220-5223. https://doi.org/10.1364/OL.471191

[7] XU Y., GUAN Y., LIU Y., LIN S., ZHU X., CAI Y., YU J., GBUR G., *Generating multi-focus beams with a spatial non-uniform coherence structure*, Optics Letters, **48**(10), 2023: 2631-2634. https://doi.org/10.1364/OL.491880

[8] WANG C., LIU L., LIU L., YU J., WANG F., CAI Y., PENG X., *Second-order statistics of a Hermite-Gaussian correlated Schell-model beam carrying twisted phase propagation in turbulent atmosphere*, Optics Express, **31**(8), 2023: 13255-13268. https://doi.org/10.1364/OE.489437

[9] LIU Y., ZHANG X., DONG Z., PENG D., CHEN Y., WANG F., CAI Y., *Robust far-field optical image transmission with structured random light beams*, Physical Review Applied, **17**(2), 2022: 024043. https://doi.org/10.1103/PhysRevApplied.17.024043

[10] FANG X.Y., REN H.R., GU M., *Orbital angular momentum holography for high-security encryption*, Nature Photonics, **14**(2), 2020: 102-108. https://doi.org/10.1038/s41566-019-0560-x

[11] YU J., XU Y., LIN S., ZHU X., GBUR G., CAI Y., *Longitudinal optical trapping and manipulating Rayleigh particles by spatial nonuniform coherence engineering*, Physical Review A, **106**(3), 2022: 033511. https://doi.org/10.1103/PhysRevA.106.033511

[12] LAJUNEN H., SAASTAMOINEN T., *Propagation characteristics of partially coherent beams with spatially varying correlations*, Optics Letters, **36**(20), 2011: 4104-4106. https://doi.org/10.1364/OL.36.004104

[13] YU J, WANG F, LIU L, CAI Y., GBUR G., *Propagation properties of Hermite non-uniformly correlated beams in turbulence*, Optics Express, **26**(13), 2018: 16333-16343. https://doi.org/10.1364/OE.26.016333

[14] BUSTAMANTE C.J., CHEMLA Y.R., LIU S., WANG M.D., *Optical tweezers in single-molecule biophysics*, Nature Reviews Methods Primers, **1**(1), 2021: 25. https://doi.org/10.1038/s43586-021-00021-6

[15] YANG Y., REN Y., CHEN M., ARITA Y., ROSALES-GUZMÁN C., *Optical trapping with structured light: A review*, Advanced Photonics, **3**(3), 2021: 034001. https://doi.org/10.1117/1.AP.3.3.034001

[16] YANG M., SHI Y., SONG Q., WEI Z., DUN X., WANG Z., WANG Z., QIU C.W., ZHANG H., CHENG X., *Optical sorting: past, present and future*, Light: Science & Applications, **14**(1), 2025: 103. https://doi.org/10.1038/s41377-024-01734-5

[17] TIAN S., CHEN X., DING B., *Manipulation of single nanowire and its applications*, Small Methods, **9**(8), 2025: 2402053. https://doi.org/10.1002/smtd.202402053

[18] ZHANG Z., AHMED D., *Light-driven high-precision cell adhesion kinetics*, Light: Science & Applications, **11**(1), 2022: 266. https://doi.org/10.1038/s41377-022-00963-w

[19] LI B., FU Q., LU Y., CHEN C., ZHAO Y., ZHAO Y., CAO M., ZHOU W., FAN X., JIANG X., ZHAO P., ZHENG Y., *3D hydrogel platform with macromolecular actuators for precisely controlled mechanical*

forces on cancer cell migration, Nature Communications, **16**(1), 2025: 4831. https://doi.org/10.1038/s41467-025-60062-3

[20] STOEV I.D., SEELBINDER B., ERBEN E., MAGHELLI N., KREYSING M., *Highly sensitive force measurements in an optically generated, harmonic hydrodynamic trap*, eLight, **1**, 2021: 7. https://doi.org/10.1186/s43593-021-00007-7

[21] ZHANG C., MUÑETÓN DÍAZ J., MUSTER A., ABUJETAS D.R., FROUFE-PÉREZ L.S., SCHEFFOLD F., *Determining intrinsic potentials and validating optical binding forces between colloidal particles using optical tweezers*, Nature Communications, **15**(1), 2024: 1020. https://doi.org/10.1038/s41467-024-45162-w

[22] ZHANG Y., LIU J., HU F., WANG Z., LIU Z., QIN Y., ZHANG Y., ZHANG J., YANG X., YUAN L., *Optical fiber tweezers: From fabrication to applications*, Optics & Laser Technology, **175**, 2024: 110681. https://doi.org/10.1016/j.optlastec.2024.110681

[23] WANG R., LI W., XIA Z., DENG H., ZHANG Y., FU R., ZHANG S., EUSER T.G., YUAN L., SONG N., JIANG Y., XIE S., *Optical trapping of mesoscale particles and atoms in hollow-core optical fibers: Principle and applications*, Light: Science & Applications, **14**(1), 2025: 146. https://doi.org/10.1038/s41377-025-01801-5

[24] ANDREWS L.C., PHILLIPS R.L., *Laser beam propagation through random media*, SPIE Press, Bellingham, 2005. https://doi.org/10.1117/3.626196

[25] ZHANG H., *Propagation of integral and fractional perfect vortex beams in a gradient-index medium,* Applied Optics, **63**(2), 2024: 492-498. https://doi.org/10.1364/AO.507662

[26] HUI Y., CUI Z., SONG P., *Propagation characteristics of non-diffracting Lommel beams in a gradient-index medium*, Waves in Random Complex Media, **31**(6), 2021: 2514-2524. https://doi.org/10.1080/17455030.2020.1758360

[27] HARADA Y., ASAKURA T., *Radiation forces on a dielectric sphere in the Rayleigh scattering regime*, Optics Communications, **124**(5-6), 1996: 529-541. https://doi.org/10.1016/0030-4018(95)00753-9

[28] CHAUMET P.C., NIETO-VESPERINAS M., *Time-averaged total force on a dipolar sphere in an electromagnetic field*, Optics Letters, **25**(15), 2000: 1065-1067. https://doi.org/10.1364/OL.25.001065

[29] OKAMOTO K., KAWATA S., *Radiation force exerted on subwavelength particles near a nanoaperture*, Physical Review Letters, **83**(22), 1999: 4534-4537. https://doi.org/10.1103/PhysRevLett.83.4534

Received August 31, 2025
in revised form November 11, 2025